

Nanoscale

Accepted Manuscript



This is an *Accepted Manuscript*, which has been through the Royal Society of Chemistry peer review process and has been accepted for publication.

Accepted Manuscripts are published online shortly after acceptance, before technical editing, formatting and proof reading. Using this free service, authors can make their results available to the community, in citable form, before we publish the edited article. We will replace this *Accepted Manuscript* with the edited and formatted *Advance Article* as soon as it is available.

You can find more information about *Accepted Manuscripts* in the [Information for Authors](#).

Please note that technical editing may introduce minor changes to the text and/or graphics, which may alter content. The journal's standard [Terms & Conditions](#) and the [Ethical guidelines](#) still apply. In no event shall the Royal Society of Chemistry be held responsible for any errors or omissions in this *Accepted Manuscript* or any consequences arising from the use of any information it contains.

Controlling the spatial arrangement of organic magnetic anions adsorbed on epitaxial graphene on Ru(0001)[†]

Daniele Stradi,^{a,b,†} Manuela Garnica,^{b,c,¶} Cristina Díaz,^a Fabián Calleja,^c Sara Barja,^{b,c} Nazario Martín,^{b,d} Manuel Alcamí,^{‡a,b} Amadeo L. Vazquez de Parga,^{b,c} Rodolfo Miranda^{b,c} and Fernando Martín^{a,b,*}

Received Xth XXXXXXXXXXXX 20XX, Accepted Xth XXXXXXXXXXXX 20XX

First published on the web Xth XXXXXXXXXXXX 200X

DOI: 10.1039/b000000x/

Achieving control over the self-organization of functional molecules on graphene is critical for the development of graphene technology in organic electronic and spintronic. Here, by using a scanning tunneling microscope (STM), we show that the electron acceptor molecule 7,7',8,8'-tetracyano-p-quinodimethane (TCNQ) and its fluorinated derivative 2,3,5,6-tetrafluoro-7,7',8,8'-tetracyano-p-quinodimethane (F4-TCNQ), co-deposited on the surface of epitaxial graphene on Ru(0001), transform spontaneously into their corresponding magnetic anions and self-organize in two remarkably different structures. TCNQ forms densely packed linear magnetic arrays, while F4-TCNQ molecules remain as isolated non interacting magnets. With the help of density functional theory (DFT) calculations, we trace back the origin of this behavior in the competition between the intermolecular repulsion experienced by the individual charged anions, which tends to separate the molecules, and the delocalization of the electrons transferred from the surface to the molecules, which promotes the formation of molecular oligomers. Our results demonstrate that it is possible to control the spatial arrangement of organic magnetic anions co-adsorbed on a surface by means of chemical substitution, paving the way for the design of two-dimensional fully organic magnetic structures on graphene and on other surfaces.

1 Introduction

Molecular functionalization^{1–12} is a promising approach to introduce new advanced functionalities in graphene¹³. Among them, organic-based magnetism¹⁴ stands out because of its potential use in spintronic applications for cost-effective and flexible semiconductor technology^{15–18}. Driven by these perspectives, the covalent functionalization of graphene by atomic¹⁹ and molecular²⁰ precursors has been successfully used to create purely organic graphene structures exhibiting stable magnetism^{21,22} even at room temperature^{23–26}.

Nevertheless, obtaining spatially ordered 2D adlayers of such magnetic interfaces still constitutes a problem, due to the high reactivity of the radical species that must be employed to functionalize the graphene monolayer^{27,28}. Consequently, the control that can be exerted during the synthesis remains limited, and the degree of long-range order in these functionalized graphene structures varies considerably depending on the precise experimental conditions^{29–33}. A feasible alternative is the non-covalent functionalization of graphene^{34,35}. In this respect, we have recently shown that the deposition of the molecular electron acceptor 7,7',8,8'-tetracyano-p-quinodimethane (TCNQ) on epitaxial graphene on Ru(0001)^{36–40} (gr./Ru(0001) for short) achieved in earlier work provides a viable route to obtain 2D ordered magnetic molecule/graphene interfaces⁴¹.

In an attempt to clarify the factors governing molecular self-organization of these non-covalent interfaces, several works have investigated the structure of self-organized molecular layers physisorbed on epitaxial 2D substrates⁴², such as graphene^{43–49} and hexagonal boron nitride (h-BN)^{50–52}. The present understanding is that, on these surfaces, π - π stacking interactions are mainly responsible for molecular adsorption, whereas molecular self-organization is the result of intermolecular interactions⁴⁷. In the presence of electronic and structural inhomogeneities, the substrate can also

[†] Electronic Supplementary Information (ESI) available: 2D PES of the neutral [TCNQ]₂ and [F4-TCNQ]₂ dimers in the gas-phase and calculated frontier orbitals of the neutral TCNQ and F4-TCNQ molecules in the gas-phase. . See DOI: 10.1039/b000000x/

^a Departamento de Química, Universidad Autónoma de Madrid, Cantoblanco 28049, Madrid, Spain. E-mail: fernando.martin@uam.es

^b Instituto Madrileño de Estudios Avanzados en Nanociencia (IMDEA-Nanociencia), Cantoblanco 28049, Madrid, Spain

^c Departamento de Física de la Materia Condensada, Univesidad Autónoma de Madrid, Cantoblanco 28049, Madrid, Spain

^d Facultad de Química, Universidad Complutense de Madrid, 28040, Madrid, Spain

[†] Present address: Department of Micro- and Nanotechnology (DTU Nanotech), Center for Nanostructured Graphene (CNG), Ørstedts Plads, Building 345E, DK-2800 Kgs. Lyngby, Denmark

[¶] Present address: TU München, Physik-Department E20, James-Frank-Str.1, D-85748 Garching

play an important role as a template^{43,44,47,49}. More importantly, on strongly interacting graphene-metal substrates, such as on gr./Ru(0001)^{37–39,53–56}, a spontaneous charging of the molecule may occur upon adsorption. In this case, the graphene also acts as a buffer layer, decoupling efficiently the molecular electronic states from those of the underlying metal. As a consequence, the magnetic properties of the charged molecules deposited on the surface are preserved, thus leading to the creation of organic magnets directly on the graphene surface starting from non-magnetic precursors⁴¹.

Here, we highlight the profound impact of chemical composition on the self-organization of two molecules, TCNQ and its fluorinated derivative 2,3,5,6-tetrafluoro-7,7',8,8'-tetracyano-p-quinodimethane (F4-TCNQ). The structures formed by the two species can be readily discriminated by using scanning tunneling microscopy (STM). TCNQ molecules form densely packed linear oligomers, whereas F4-TCNQ molecules remain isolated, arranging in a sparse pattern over the low areas of the graphene moiré. This behavior remains unaltered upon co-adsorption of both species. Density functional theory (DFT) calculations are used to rationalize the experimental observations, showing that (i) the two adsorbed molecules share similar charge transfer and magnetic properties, and that (ii) the intermolecular delocalization of the transferred electrons is the key factor determining the self-organization behavior observed experimentally. Due to the favorable overlap between the electronic clouds of the neighboring molecules, electron delocalization stabilizes energetically the charged TCNQ oligomers on the surface, whereas a much less favorable overlap in the case of the charged F4-TCNQ molecules prevents an efficient electronic delocalization, so that intermolecular repulsion prevails.

2 Experimental methods

The experiments have been carried out in an ultra-high vacuum (UHV) chamber with a base pressure of 1×10^{-11} mbar, equipped with standard facilities for surface preparation and characterization, low energy electron diffraction (LEED) and a low temperature scanning tunneling microscope (STM) working at 4.6K. Ultra-perfect gr./Ru(0001) substrates have been grown by thermal decomposition of ethylene on Ru(0001) as described in Ref. 37. The molecules have been deposited at room temperature and subsequently the sample has been cooled down to 4.6 K to achieve stable STM imaging.

3 Computational methods

Theoretical calculations have been performed using density functional theory (DFT). The electronic exchange-correlation energy has been described using the generalized gradient ap-

proximation (GGA) and the Perdew-Burke-Ernzerhof (PBE) functional⁵⁷, employing the DFT+D2 semi-empirical correction of Grimme⁵⁸ to account for van der Waals interactions. In the case of the isolated monomers adsorbed on the gr./Ru(0001) surface and for the calculations of the potential energy surfaces (PESs) of the molecular dimers, calculations have been performed using VASP⁵⁹. The ionic cores have been described by using the projector augmented waves (PAW) method⁶⁰. The kinetic energy cutoff for the plane-waves expansion has been set to 400 eV and the Brillouin zone has been sampled at Γ -point. A Methfessel-Paxton smearing⁶¹ of 0.1 eV and a Gaussian smearing of 0.1 eV have been used during the calculation of the monomers adsorbed on gr./Ru(0001) and of the PESs of the dimers, respectively. The surface of gr./Ru(0001) has been described using a model formed by 11×11 graphene unit cells matched to a three-layer metallic slab formed by 10×10 Ru(0001) unit cells³⁸, with a vacuum gap between the periodically repeated images in the z direction of 10.2 Å. This structure has been shown to reproduce correctly most of the features observed experimentally on this surface using the STM^{38,39}. The structure of the isolated monomers on the surface has been optimized using a convergence threshold for the forces of 2.5×10^{-2} eV/Å. During the geometry optimization, the molecular degrees of freedom have been allowed to relax, whereas the atoms of the surface have been kept fixed. Spin-polarized DFT calculations have been performed on the DFT optimized structures. STM topographs have been simulated using the Tersoff-Hamman approximation⁶². The electronic density redistribution $\Delta\rho(\mathbf{r})$ due to the adsorption of each molecule on gr./Ru(0001) has been calculated as $\Delta\rho(\mathbf{r}) = \rho_{mol.+gr./Ru(0001)}(\mathbf{r}) - [\rho_{mol.}(\mathbf{r}) + \rho_{gr./Ru(0001)}(\mathbf{r})]$, where $\rho_{mol.+gr./Ru(0001)}(\mathbf{r})$ is the ground state electronic density of the adsorbed molecule, and $\rho_{mol.}(\mathbf{r})$ and $\rho_{gr./Ru(0001)}(\mathbf{r})$ are the electronic densities of the two non-interacting fragments - *i.e.*, the molecule and the gr./Ru(0001) substrate with their respective geometries kept frozen at those of the ground state of the combined system.

The PES of the molecular dimers in the gas phase has been sampled by varying the radial coordinate d (*i.e.*, the distance between the centers of mass of the molecules) and azimuthal angle Θ , (*i.e.*, the angle formed between the vectors connecting the two centers of mass and the x axis), using regular steps $\Delta d = 0.2$ Å and $\Delta\Theta = 2^\circ$, with the molecules placed in a 40 Å \times 40 Å \times 10 Å box, lying on the same plane and having the long (short) axis oriented along the y (x) axis.

Additional calculations for the neutral, singly charged and doubly charged monomers and dimers in the gas-phase have been carried out with Gaussian09⁶³, using the PBE functional and a 6-311G++(d,p) basis set. Tests performed on the gas-phase monomers and dimers using the hybrid B3LYP⁶⁴ functional lead to results almost identical to the PBE ones (see

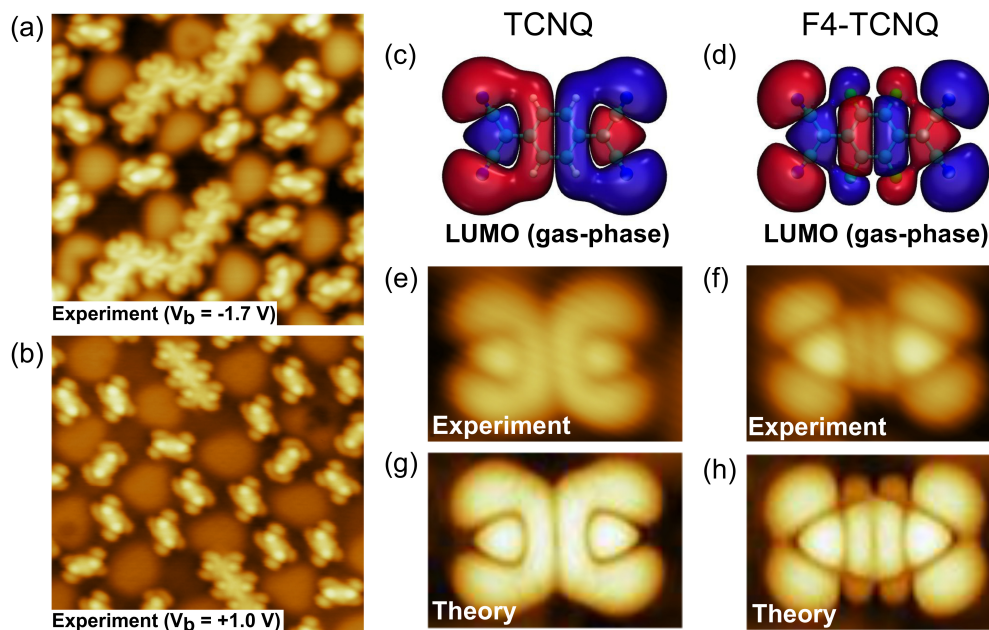


Fig. 1 (a) STM topography ($10 \times 10 \text{ nm}^2$) of TCNQ and F4-TCNQ co-adsorbed on gr./Ru(0001). Parameters: $V_b = -1.7 \text{ V}$, $I_t = 10 \text{ pA}$. (b) Same as (a) but at positive bias voltages. Parameters: $V_b = +1.0 \text{ V}$, $I_t = 10 \text{ pA}$. (c) LUMO of the neutral TCNQ molecule calculated in the gas-phase. The wave function is colored according to its negative (red) and positive (blue) sign. (e) High resolution STM topographies ($3 \times 3 \text{ nm}^2$) of an individual TCNQ molecule adsorbed on gr./Ru(0001), taken at negative bias voltage (Parameters: $V_b = -0.3 \text{ V}$, $I_t = 50 \text{ pA}$). (g) Simulated STM image of an isolated TCNQ molecule adsorbed on gr./Ru(0001) at negative bias voltage (Integration range: $-0.3 \text{ eV} \leq E - E_F \leq 0.0 \text{ eV}$). (d,f,h) Same as (c,e,g), but for F4-TCNQ. Carbon, nitrogen, fluorine and hydrogen atoms are shown in cyan, blue, green and white, respectively.

Table S1 in the Supplementary Information).

4 Results and discussion

Gr./Ru(0001) presents a moiré superstructure with a periodicity of $\sim 30 \text{ \AA}$, due to the mismatch between the lattice constant of graphene ($a_{\text{gr.}} = 2.46 \text{ \AA}$) and that of Ru(0001) ($a_{\text{Ru(0001)}} = 2.7 \text{ \AA}$)^{36,37,40,54,65,66}. These periodic variations create a geometric buckling of the surface and a modulated potential energy landscape^{37,39,56}, which has been shown to be responsible for inducing selective molecular adsorption on defined regions of the graphene moiré^{41,43–46,48}. A STM topography of TCNQ and F4-TCNQ co-adsorbed on gr./Ru(0001) is presented in Fig. 1(a), showing that the molecules adsorb exclusively over the low regions of the moiré, where the surface potential is $\sim 0.25 \text{ eV}$ lower⁶⁷. The molecular arrangement is strikingly different for TCNQ and F4-TCNQ: while the TCNQ molecules assemble in dense linear chains across the low regions of the moiré, the F4-TCNQ molecules remain isolated, and arrange in a sparse configuration in which every molecule lies approximatively at the center of each low region.

Figures 1(c) and 1(d) show the lowest unoccupied molecu-

lar orbital (LUMO) of the two neutral monomers in the gas-phase. A common feature is the presence of a central node along the short axis of both molecules, which is not present in the highest occupied molecular orbitals (HOMO) (see Figure S2 in the Supplementary Information). Due to the presence of a much larger number of nodes in the F4-TCNQ frontier molecular orbitals compared to that of TCNQ, the two different species can be simply recognized by comparing the high resolution STM topographs measured over individual TCNQ (Fig. 1(e)) and F4-TCNQ (Fig. 1(f)) monomers⁶⁸. The corresponding STM simulations using the optimized structures of the isolated molecules on gr./Ru(0001) resulting from elaborate DFT calculations (Fig. 1(g,h)) are in excellent agreement with the experiment, thereby excluding that this difference is an artifact due to the limited experimental resolution. Even in the large-scale STM image presented in Fig. 1(a), these topographical features can still be recognized. This indicates that the graphene acts as an efficient buffer layer for both the TCNQ and the F4-TCNQ adsorbates.

The topographs shown in Fig. 1(e-h) resemble closely the LUMO of the two neutral monomers in the gas-phase (see Fig. 1(c,d)). At the same time, they differ considerably from the

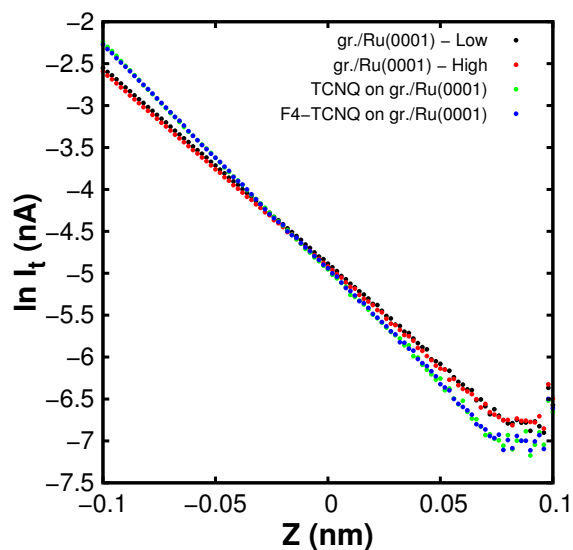


Fig. 2 Plot of $\ln I_t$ as a function of the tip displacement Z . Black and red data points are relative to the spectra measured at the Low and High regions of the clean gr./Ru(0001) moiré, respectively. Green and blue data points are relative to the spectra measured above the adsorbed TCNQ and F4-TCNQ molecules, respectively.

rest of the orbitals lying close in energy to the LUMO, *i.e.* the LUMO+1 and the HOMO (see Figure S2 in the Supplementary Information). However, the STM experiments and the corresponding simulations are probing the occupied electronic structure of the sample at $V_{\text{bias}} < 0$ V, which suggests that in both molecules the LUMO has been occupied by electrons upon adsorption on the surface. Furthermore, topographs with similar features are observed also at $V_{\text{bias}} > 0$ V (see Figure 1(b)), indicating that the LUMO is only partially occupied. In the case of TCNQ, this picture has been confirmed by scanning tunneling spectroscopy (STS) and DFT calculations, and XPS measurements⁶⁹, which have shown that one entire electron is transferred from the surface to the LUMO of the neutral molecule upon adsorption on gr./Ru(0001) ⁴¹. In the present case, the existence of electron transfer has been confirmed using STS. dI/dZ measurements indicate that the local potential, calculated from the slope of the $\ln I_t$ vs. Z curves (see Fig. 2), is -5.03 eV and -5.16 eV at the low and at the high regions of the clean gr./Ru(0001) moiré, respectively. This variation is in line with the difference in local potential obtained by photoemission of adsorbed Xenon⁶⁷. However, in the vicinity of each molecule, the local potential is -6.51 eV (TCNQ) and -6.48 eV (F4-TCNQ). This marked change in the local potential, with respect to that of the clean surface, is due to the presence of a local dipole normal to the surface, which develops as a consequence of the electron transfer from the surface to the

Table 1 Adsorption energy ($E_{\text{ads.}}$), adsorption distance ($z_{\text{ads.}}$), Charge state (Q) and integrated spin density (S) of the individual TCNQ and F4-TCNQ molecules adsorbed on the Hcp-Top, Fcc-Top and Bridge (*i.e.*, in between Hcp-Top and Fcc-Top) low areas of gr./Ru(0001) .

	TCNQ		F4-TCNQ	
	0°	30°	0°	30°
Hcp-Top				
$E_{\text{ads.}}$ (eV)	-2.48	-2.53	-3.10	-3.09
$z_{\text{ads.}}$ (Å)	3.07	3.05	3.07	3.04
Q (nr. e^-)	1.02	1.02	1.22	1.24
S (μ_B)	0.09	0.26	0.23	0.27
Bridge				
$E_{\text{ads.}}$ (eV)	-2.45	-2.47	-3.05	-3.05
$z_{\text{ads.}}$ (Å)	3.06	3.04	3.06	3.06
Q (nr. e^-)	0.99	0.98	1.20	1.20
S (μ_B)	0.36	0.38	0.43	0.29
Fcc-Top				
$E_{\text{ads.}}$ (eV)	-2.38	-2.37	-2.97	-2.96
$z_{\text{ads.}}$ (Å)	3.06	3.04	3.07	3.04
Q (nr. e^-)	0.96	0.98	1.21	1.18
S (μ_B)	0.86	0.97	0.62	0.69

molecule. The present results indicate that the charge transfer characteristics of F4-TCNQ adsorbed on gr./Ru(0001) are likely to be similar to those of TCNQ.

Indeed, according to our DFT calculations, the F4-TCNQ monomer adsorbed on gr./Ru(0001) behaves similarly to TCNQ (see Table 1). Both molecules lie almost flat on the surface, at a distance $z_{\text{ads.}} \sim 3$ Å, indicative of a weak molecule-substrate interaction. This agrees with the fact that, in the STM experiments, they can be easily displaced from their equilibrium position, if electronic currents of the order of $I_t \sim 0.3$ nA are applied. Furthermore, albeit the calculated average adsorption energy ($E_{\text{ads.}}$) for F4-TCNQ is about 0.5 eV larger than for TCNQ, the difference in $E_{\text{ads.}}$ within each low area of the graphene moiré is very small ($\Delta E_{\text{ads.}} < 20$ meV) for both molecules, confirming that TCNQ⁴¹ and F4-TCNQ show no preference for a particular adsorption configuration on gr./Ru(0001) . An analysis of the electronic density based on the quantum theory of atoms in molecules^{72,73} (QTAIM) shows that each F4-TCNQ molecule receives on average 1.21 electrons (e^-) from the substrate, a value that is only a slightly larger than that calculated for the TCNQ molecule, 0.99 e^- . For the latter, it has been shown that the charge transfer leads to the appearance of a sizable magnetic moment localized on

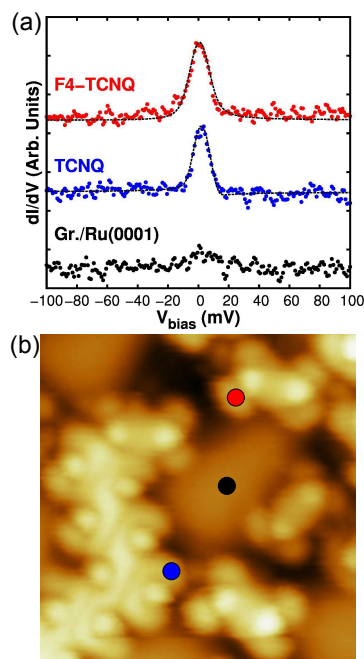


Fig. 3 (a) Differential conductance, dI/dV , spectra measured with a lock-in technique ($V_{\text{mod}}=14$ mV RMS and $\nu=703$ Hz) and the STM tip positioned above the high region of gr./Ru(0001) (black curve), and above the cyano group of a TCNQ molecule (blue curve) and of a F4-TCNQ molecule (red curve) co-adsorbed on the surface. The dashed black lines superimposed to each curve are the corresponding fits using a Fano line shape⁷⁰, $(q + \varepsilon)^2 / (1 + \varepsilon^2)$, where q is the asymmetry parameter and $\varepsilon = (V_b - V_{\text{res}}) / (\Gamma/2)$, with Γ being the resonance width, V_b the bias voltage and V_{res} the bias voltage at which the resonance has its maximum. Fitting parameters: $q = -10$, $\Gamma = 4$ mV, $V_{\text{res}} = 3$ mV (TCNQ) and $q = 40$, $\Gamma = 8$ mV, $V_{\text{res}} = 0.5$ mV (F4-TCNQ). (b) Topographic STM image (5×5 nm², Parameters: $V_b = -0.2$ V, $I_t = 50$ pA) of the TCNQ and of the F4-TCNQ molecules co-adsorbed on gr./Ru(0001). The dots superimposed to the image indicate the position where the spectra shown in (a) have been measured.

the molecule⁴¹. The present spin-polarized DFT calculations predict a similar behavior for F4-TCNQ (see Table 1). Therefore, DFT predicts that both TCNQ and F4-TCNQ behave as magnetic anions when they are adsorbed on the surface of gr./Ru(0001).

For individual TCNQ and F4-TCNQ species deposited on gr./Ru(0001), the appearance of a magnetic moment on the molecule, due to a charge transfer upon adsorption, has been confirmed experimentally by scanning tunneling spectroscopy (STS) measurements. The latter have revealed the presence of a sharp feature at $V_{\text{bias}} = 0$ V, associated with the formation of a Kondo state between the unpaired electron residing on the negatively charged molecule, and the conduction electrons of the metallic surface underneath^{41,74}. A similar picture

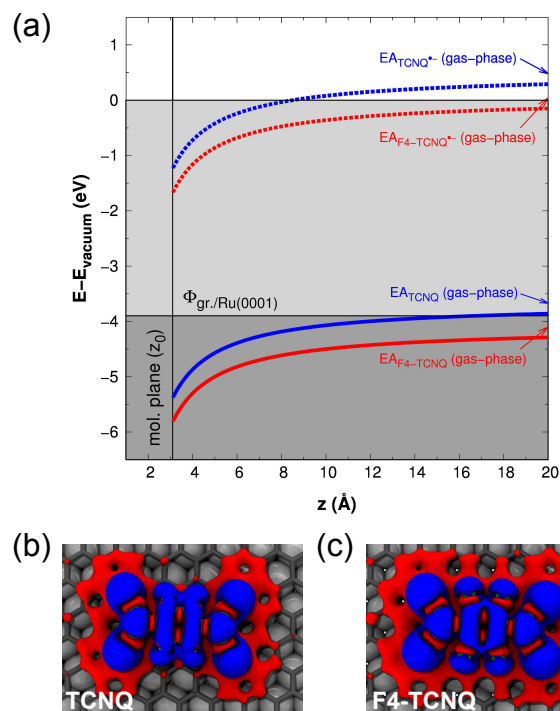


Fig. 4 (a) Change in the 1st electron affinity (EA) of TCNQ (solid blue line), TCNQ^{•-} (dashed blue line), F4-TCNQ (solid red line) and F4-TCNQ^{•-} (dashed red line), due to the image charge effect. $z = 0.0$ Å indicates the surface plane of gr./Ru(0001). $z_0 = 3.0$ Å indicates the molecular plane of the adsorbed molecules. The image plane is set at $z = 1.0$ Å⁷¹. The arrows on the left side of the image indicate the values of EA for the molecules in the gas phase (*i.e.*, $z \rightarrow \infty$). The energy E on the Y axis is scaled with respect to the vacuum level E_{vacuum} . (b,c) Top view of the isosurface (isovalue = $1.0 \times 10^{-4} e^-/\text{Å}^3$) indicating the electronic density redistribution $\Delta\rho$ upon the adsorption of TCNQ (b) and F4-TCNQ (c) on gr./Ru(0001). Blue and red colors indicate electron accumulation ($\Delta\rho > 0.0 e^-/\text{Å}^3$) and electron depletion ($\Delta\rho < 0.0 e^-/\text{Å}^3$), respectively.

also persists when the two molecules are co-adsorbed on the surface. Figure 3 (a) shows STS spectra measured on the co-adsorbed molecular layer in a narrow range around $V_{\text{bias}} = 0$ V. While the spectrum measured over the clean gr./Ru(0001) is essentially featureless, those measured over both molecules show the presence of a sharp Kondo peak at $V_{\text{bias}} \sim 0$ V. By fitting the peaks with a Fano line shape⁷⁰ we obtain $q = -10$ (TCNQ) and $q = 40$ (F4-TCNQ). These large values of q suggest that the molecule-surface coupling is weak⁴¹. From the width Γ of the fitted data we estimate the Kondo temperature to be $T_K = 58$ K and $T_K = 70$ K for the adsorbed TCNQ and F4-TCNQ molecules, respectively. The value of T_K obtained for TCNQ is similar to that obtained for the same molecule adsorbed, either isolated or at 0.5 ML coverage, on

gr./Ru(0001) in the absence of F4-TCNQ^{41,74}. These results confirm that the magnetic character of both TCNQ and F4-TCNQ is preserved upon co-adsorption of the two molecules on gr./Ru(0001).

Using simple qualitative arguments, it is possible to understand why charge transfer due to adsorption on gr./Ru(0001) is similar for TCNQ and F4-TCNQ, despite the presence of strongly electron-withdrawing fluorine atoms in the latter. In the gas-phase, the addition of an electron to either TCNQ or F4-TCNQ is a favorable process, as their 1st electron affinity (EA), calculated as the difference between the total energies of the neutral molecule and of the singly charged anion⁷⁵, is -3.67 eV⁷⁶ and -4.01 eV, respectively. Conversely, the formation of the doubly charged anions is unfavorable, as indicated by the calculated EAs of the two singly charged anions, 0.48 eV and 0.04 eV, respectively. The EAs of the neutral species in the *vacuum* thus lie close to the work function of gr./Ru(0001), $\Phi_{\text{gr./Ru(0001)}} = -3.9$ eV^{55,67}, whereas the EAs of the two radical anions are very far in energy from $\Phi_{\text{gr./Ru(0001)}}$. As the molecules approach gr./Ru(0001), the mutual polarization between the electronic clouds of the molecule and of the surface shifts the EAs to more negative values. In the limit of a weak molecule-substrate interaction, the leading correction term to such change can be estimated using a classical image charge model, *i.e.* by considering the interaction of a point-like charge with a flat conducting surface^{71,77}, $E_{\text{image}} = -1/4(z - z_0)$, where z and z_0 are the position of the molecular center of mass and of the image plane with respect to the surface, respectively. Already at relatively large values of z , the proximity of the surface leads to a large drop in the EAs of the two neutral species, so that they both fall below $\Phi_{\text{gr./Ru(0001)}}$ (see Fig. 4(a)). At $z = 3.0$ Å, which corresponds approximately to the calculated values of z_{ads} , the Fermi energy of the metal lies well above the EAs of the neutral molecules, and a spontaneous electron transfer from the surface to the molecule occurs, resulting in a singly-charged molecular anion. The shift induced by the image charge in the latter anions is not sufficient to bring the EAs of TCNQ^{•-} and F4-TCNQ^{•-} below $\Phi_{\text{gr./Ru(0001)}}$, thus hindering the full occupation of the LUMO of the neutral molecules.

A more detailed insight into the charge transfer process outlined above can be obtained by considering the electronic density redistribution $\Delta\rho(\mathbf{r})$ due to the adsorption of each molecule on gr./Ru(0001). For both molecules, an analysis of the spatial distribution of $\Delta\rho(\mathbf{r})$ shows that the electronic density accumulated on the molecule comes from the surface underneath (see Fig. 4(b,c)). The number and position of the nodes in the region of $\Delta\rho(\mathbf{r}) > 0.0$ e⁻/Å³, which is completely localized on the molecule, match those of the LUMOs of TCNQ and F4-TCNQ, further supporting the idea that the electronic charge that has been removed from the surface goes into the LUMO of the neutral molecules. A closer in-

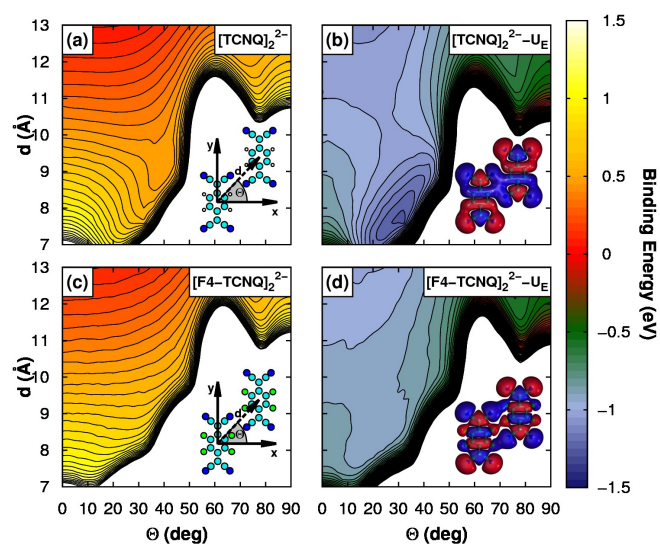


Fig. 5 2D potential energy surfaces (PESs) of [TCNQ]₂²⁻ (a) and [TCNQ]₂²⁻-U_E (b), as a function of the distance d and the intermolecular angle Θ between the center of mass of the two molecules - see inset in (a). The separation between each isodensity curve is 5.0×10^{-2} eV. The inset in (b) shows the LUMO of [TCNQ]₂²⁻-U_E at $d = 8.0$ Å and $\Theta = 34^\circ$. (c,d) Same as (a,b), but for [F4-TCNQ]₂²⁻ and [F4-TCNQ]₂²⁻-U_E. Carbon, nitrogen, fluorine and hydrogen atoms are shown in cyan, blue, green and white, respectively. In the inset in (b,d) the wavefunction is colored according to its negative (red) and positive (blue) sign.

spection also reveals that the position of the nodes coincides with regions located close to the molecular skeleton at which $\Delta\rho(\mathbf{r}) < 0.0$ e⁻/Å³, indicating that a smaller fraction of electronic density is also depleted from the molecular σ system. Overall, the shape of $\Delta\rho(\mathbf{r})$ is indicative of a donation mechanism reminiscent of that observed for TCNQ on Cu(100)⁷⁸ and F4-TCNQ on Cu(111)⁷⁹, although in the present case the amount of charge transfer is smaller, due to the weaker bonding of the molecule with the surface.

The isolated monomers of TCNQ and F4-TCNQ adsorbates thus behave very similarly on gr./Ru(0001). However, as shown in the following, the interaction between the charged anions adsorbed on the surface is considerably different and can be regarded as the driving force for the formation of the self-organized structures observed experimentally. For this purpose, we have performed DFT calculations for the doubly-charged [TCNQ]₂²⁻ and [F4-TCNQ]₂²⁻ dimers in the gas-phase⁸⁰. Fig. 5(a,c) shows the corresponding 2D potential energy surfaces (PESs). As expected, the two PESs are completely repulsive. This implies that, in the gas-phase, the individual monomers of [F4-TCNQ]₂²⁻, as well as those of [TCNQ]₂²⁻, will move away one from each other due to the strong intermolecular repulsion, in contrast to the experimen-

tal observations for the molecules adsorbed on gr./Ru(0001). Including explicitly the presence of the substrate in the evaluation of the PESs is thus crucial to realistically describe the behavior of the anions upon adsorption. In particular, one can expect the conductive gr./Ru(0001) surface to screen the extra charge present on the charged monomers, thus diminishing the intermolecular electrostatic repulsion and favoring aggregation. To estimate this effect, we have considered the limit case in which the classical electrostatic energy $U_E(d)$ due to the interaction between two identical point charges Q separated by a distance d , $U_E(d) = Q^2/(4\pi\epsilon_0 d)$, is removed from the calculated gas-phase PESs.

As can be seen, removing this electrostatic repulsion has dramatic consequences on the qualitative behavior of the two PESs (see Fig. 5(b,d)): the new PES for the screened $[\text{TCNQ}]_2^{2-}$, hereafter called $[\text{TCNQ}]_2^{2-}-U_E$, exhibits a well defined minimum at $d \sim 8 \text{ \AA}$ and $\Theta \sim 34^\circ$, whereas that for the screened $[\text{F4-TCNQ}]_2^{2-}$, hereafter called $[\text{F4-TCNQ}]_2^{2-}-U_E$, does not present any minimum around that region. The corrected PESs are very similar to those for the corresponding neutral dimers (see Supplementary Information). The results of this simple model are compatible with the experimental observations: while F4-TCNQ molecules tend to separate from each other even in the absence of any repulsive Coulomb interaction between them, TCNQ molecules prefer staying close to each other at a distance d and angle Θ similar to those found in the experiment or the full calculation⁴¹. The remarkable differences between the PESs of the $[\text{TCNQ}]_2^{2-}-U_E$ and $[\text{F4-TCNQ}]_2^{2-}-U_E$ systems are a direct consequence of the presence of the F atoms, which have electron pairs that repel when confronted in the dimer with N or other F atoms. At small values of d , where Pauli repulsion is expected to determine the differences between the two PESs, this effect should lead to a larger intermolecular repulsion for $[\text{F4-TCNQ}]_2^{2-}$ than for $[\text{TCNQ}]_2^{2-}$. This is indeed the behavior that can be observed by comparing Figure 5(a) and Figure 5(c) around the relevant values of d and Θ . Furthermore, this influences the nodal structure of the frontier orbitals of the two anions. In fact, the HOMO of $[\text{TCNQ}]_2^{2-}-U_E$, calculated at the position of the minimum, is completely node-less in the region in between the two TCNQ^- monomers (see the inset in Fig. 5(b)), whereas the HOMO of $[\text{F4-TCNQ}]_2^{2-}-U_E$, calculated at the same values of d and Θ , exhibits a number of nodes in the same region (see the inset in Fig. 5(d)). Consequently, electrons occupying the HOMO of $[\text{TCNQ}]_2^{2-}-U_E$ are more efficiently delocalized over the two molecules than those occupying the HOMO of $[\text{F4-TCNQ}]_2^{2-}-U_E$. This makes the PES of $[\text{TCNQ}]_2^{2-}-U_E$ more attractive than that of $[\text{F4-TCNQ}]_2^{2-}-U_E$. The same effect explains the self-organization behavior of TCNQ and F4-TCNQ co-adsorbed on gr./Ru(0001). For TCNQ, the overlap between the frontier orbitals of the neighboring molecules is sufficient to promote the delocalization of the electrons trans-

ferred from the surface over the whole oligomers, thus diminishing the intermolecular repulsion between the charged fragments and favoring their aggregation in the low regions of the gr./Ru(0001) moiré. Conversely, for F4-TCNQ, this condition is not achieved, so that the charged anions tend to minimize the intermolecular repulsion by separating from each other as much as possible, thus forming the sparse pattern observed in the STM experiments.

5 Conclusions

In conclusion, scanning tunneling microscopy (STM) experiments have been employed to show that co-deposition of the organic electron acceptor TCNQ and its fluorinated derivative F4-TCNQ on the surface of epitaxial graphene on Ru(0001) results in the formation of two distinct self-organized structures, characterized by a dense (sparse) arrangement of the TCNQ (F4-TCNQ) molecules. Density functional theory (DFT) calculations show that, as confirmed by scanning tunneling spectroscopy (STS) measurements, F4-TCNQ, similarly to TCNQ⁴¹, develops a finite magnetic moment upon co-adsorption due to electron transfer from the surface, and reveal that the organization behavior observed experimentally for the two molecules is due to the high (low) efficiency with which these extra electrons are delocalized across neighboring TCNQ (F4-TCNQ) molecules. Controlling electron delocalization by means of chemical substitution thus allows one to engineer the spatial arrangement of 2D heteromolecular structures of organic nanomagnets deposited on the surface of epitaxial 2D systems.

6 Acknowledgement

All calculations were performed at the Red Española de Supercomputación and the Centro de Computación Científica of UAM. Financial support by the Ministerio de Educación y Ciencia through projects CONSOLIDER-INGENIO 2010 on Molecular Nanoscience, FIS2010-18847, FIS2010-15127, FIS2012-33011 and CTQ2010-17006, FIS1013-40667-P and Comunidad de Madrid through the programme NANOBIO-MAGNET S2009/MAT1726 is gratefully acknowledged. S.B. would like to acknowledge the FPU Grant AP-2007-001157. M.G. would like to acknowledge the FPI-UAM programme. D.S. would like to acknowledge support from the FPI-UAM program and from the Center for Nanostructured Graphene (CNG).

References

- 1 V. Georgakilas, M. Otyepka, A. B. Bourlinos, V. Chandra, N. Kim, K. C. Kemp, P. Hobza, R. Zboril and K. S. Kim, *Chem. Rev.*, 2012, **112**, 6156–6214.

- 2 H. Y. Mao, Y. H. Lu, J. D. Lin, S. Zhong, A. T. S. Wee and W. Chen, *Prog. Surf. Sci.*, 2013, **2**, 132–159.
- 3 D. Jariwala, V. K. Sangwan, L. J. Lauhon, T. J. Marksab and M. C. Hersam, *Chem. Soc. Rev.*, 2013, **42**, 2842.
- 4 L. Rodríguez-Pérez, M. A. Herranz and N. Martín, *Chem. Commun.*, 2013, **49**, 3721.
- 5 Y. H. Lu, W. Chen, Y. P. Feng and P. M. He, *J. Phys. Chem. B*, 2009, **113**, 2–5.
- 6 W. Chen, S. Chen, D. C. Qi, X. Y. Gao and A. T. S. Wee, *J. Am. Chem. Soc.*, 2007, **129**, 10418–10422.
- 7 C. Coletti, C. Riedl, D. Lee, B. Krauss, L. Patthey, K. von Klitzing, J. Smet and U. Starke, *Phys. Rev. B*, 2010, **81**, 235401.
- 8 D. B. Farmer, R. Golizadeh-Mojarad, V. Perebeinos, Y.-M. Lin, G. S. Tulevski, J. C. Tsang and P. Avouris, *Nano Lett.*, 2009, **9**, 388–392.
- 9 J. T. Sun, Y. H. Lu, W. Chen, Y. P. Feng and A. T. S. Wee, *Phys. Rev. B*, 2010, **81**, 155403.
- 10 J. Choi, H. Lee, K.-J. Kim, B. Kim and S. Kim, *J. Phys. Chem. Lett.*, 2010, **1**, 505.
- 11 T. O. Wehling, K. S. Novoselov, S. V. Morozov, E. E. Vdovin, M. I. Katsnelson, A. K. Geim and A. I. Lichtenstein, *Nano Lett.*, 2008, **8**, 173–177.
- 12 H. Liu, Y. Liu and D. Zhu, *J. Mater. Chem.*, 2011, **21**, 3335–3345.
- 13 A. H. Castro Neto, F. Guinea, N. M. R. Peres, K. S. Novoselov and A. K. Geim, *Rev. Mod. Phys.*, 2009, **81**, 109.
- 14 S. J. Blundell and F. L. Pratt, *J. Phys. Condens. Matter*, 2004, **16**, R771–R828.
- 15 Z. H. Xiong, D. Wu, Z. V. Vardeny and J. Shi, *Nature*, 2004, **427**, 821.
- 16 W. J. M. Naber, S. Faez and W. G. van der Wiel, *J. Phys. D: Appl. Phys.*, 2007, **40**, R205–R208.
- 17 C. Boehme and J. M. Lupton, *Nat. Nanotech.*, 2013, **8**, 612–615.
- 18 A. Schlierf, P. Samorí and V. Palermo, *J. Mater. Chem. C*, 2014, doi:10.1039/C3TC32153C.
- 19 J. E. Johns and M. E. Hersam, *Acc. Chem. Res.*, 2013, **46**, 77–86.
- 20 J. Park and M. Yan, *Acc. Chem. Res.*, 2013, **46**, 181–189.
- 21 L. Jing, P. Huang, H. Zhu and X. Gao, *Small*, 2013, **2**, 306.
- 22 J. Hong, S. Niyogi, E. Bekyarova, M. E. Itkis, P. Ramesh, N. Amos, D. Litvinov, C. Berger, W. A. de Heer, S. Khizroev and R. C. Haddon, *Small*, 2011, **9**, 1175–1180.
- 23 J. Zhou, Q. Wang, Q. Sun, X. Chen, Y. Kawazoe and P. Jena, *Nano Lett.*, 2009, **9**, 3867.
- 24 L. Xie, X. Wang, J. Lu, Z. Ni, Z. Luo, H. Mao, R. Wang, Y. Wang, H. Huang, D. Qi, R. Liu, T. Y. Z. Shen, T. Wu, H. Peng, B. Ozyilmaz, K. Loh and A. Wee, *Appl. Phys. Lett.*, 2011, **98**, 193113.
- 25 J. Hong, E. Bekyarova, P. Liang, W. A. de Heer, R. C. Haddon and S. Khizroev, *Sci. Rep.*, 2012, **2**, 624.
- 26 J. Hong, E. Bekyarova, W. A. de Heer, R. C. Haddon and S. Khizroev, *ACS Nano*, 2013, **7**, 10011–10022.
- 27 S. Niyogi, E. Bekyarova, J. Hong, S. Khizroev, C. Berger, W. de Heer and R. C. Haddon, *J. Phys. Chem. Lett.*, 2011, **2**, 2487.
- 28 G. L. C. Paulus, Q. H. Wang and M. S. Strano, *Acc. Chem. Res.*, 2013, **46**, 160–170.
- 29 Q. H. Wang, Z. Jin, K. K. Kim, A. J. Hilmer, G. L. C. Paulus, C.-J. Shih, M.-H. Ham, J. D. Sanchez-Yamagishi, K. Watanabe, T. Taniguchi, J. Kong, P. Jarillo-Herrero and M. S. S. Strano, *Nat. Chem*, 2012, **4**, 724–732.
- 30 M. E. Bekyarovas, P. Ramesh, C. Berger, M. Sprinkle, W. A. de Heer and R. C. Haddon, *J. Am. Chem. Soc.*, 2009, **131**, 1336–1337.
- 31 M. Z. Hossain, M. A. Walsh and M. C. Hersam, *J. Am. Chem. Soc.*, 2010, **132**, 15399–15403.
- 32 J. M. Englert, C. Dotzer, G. Yang, M. Schmid, C. Papp, J. M. Gottfried, H.-P. Steinrueck, E. Spiecker, F. Hauke and A. Hirsch, *Nat. Chem.*, 2011, **3**, 279–286.
- 33 C.-J. Shih, Q. H. Wang, Z. Jin, G. L. C. Paulus, D. Blankschtein and P. J. H. M. S. Strano, *Nano Lett.*, 2013, **13**, 809–817.
- 34 J. A. Mann and W. R. Dichtel, *J. Phys. Chem. Lett.*, 2013, **4**, 2649–2657.
- 35 Z. Zhang, H. Huang, X. Yang and L. Zang, *J. Phys. Chem. Lett.*, 2011, **2**, 2897–2905.
- 36 P. W. Sutter, J.-I. Flenge and E. A. Sutter, *Nat. Mater.*, 2008, **7**, 406.
- 37 A. L. Vázquez de Parga, F. Calleja, B. Borca, M. C. G. Passeggi Jr., J. J. Hinarejos, F. Guinea and R. Miranda, *Phys. Rev. Lett.*, 2008, **100**, 056807.
- 38 D. Stradi, S. Barja, C. Díaz, M. Garnica, B. Borca, J. J. Hinarejos, D. Sánchez-Portal, M. Alcamí, A. Arnau, A. L. Vázquez de Parga, R. Miranda and F. Martín, *Phys. Rev. Lett.*, 2011, **106**, 186102.
- 39 D. Stradi, S. Barja, C. Díaz, M. Garnica, B. Borca, J. J. Hinarejos, D. Sánchez-Portal, M. Alcamí, A. Arnau, A. L. Vázquez de Parga, R. Miranda and F. Martín, *Phys. Rev. B*, 2012, **85**, 121404(R).
- 40 W. Moritz, B. Wang, M. L. Bocquet, T. Brugger, T. Greber and J. Winterlin, *Phys. Rev. Lett.*, 2010, **104**, 136102.
- 41 M. Garnica, D. Stradi, S. Barja, F. Calleja, C. Díaz, M. Alcamí, N. Martín, A. L. Vázquez de Parga, F. Martín and R. Miranda, *Nat. Phys.*, 2013, **9**, 368–374.
- 42 J. M. MacLeod and F. Rosei, *Small*, 2013, **Article in print**.
- 43 J. Mao, H. Zhang, Y. Jiang, Y. Pan, M. Gao, W. Xiao and H.-J. Gao, *J. Am. Chem. Soc.*, 2009, **131**, 14136.
- 44 M. Roos, D. Künzel, B. Uhl, H.-H. Huang, O. B. Alves, H. E. Hoster, A. Gross and R. J. Behm, *J. Am. Chem. Soc.*, 2011, **133**, 9208.
- 45 H. G. Zhang, J. T. Sun, T. Low, L. Z. Zhang, Y. Pan, Q. Liu, J. H. Mao, H. T. Zhou, H. M. Guo, S. X. Du, F. Guinea and H.-J. Gao, *Phys. Rev. B*, 2011, **84**, 245436.
- 46 K. Yang, W. D. Xiao, Y. H. Jiang, H. G. Zhang, L. W. Liu, J. H. Mao, H. T. Zhou, S. X. Du and H.-J. Gao, *J. Phys. Chem. C*, 2012, **116**, 14052–14056.
- 47 S. Barja, M. Garnica, J. J. Hinarejos, A. L. Vázquez de Parga, N. Martín and R. Miranda, *Chem. Comm.*, 2010, **46**, 8198–8200.
- 48 H. T. Zhou, J. H. Mao, G. Li, Y. L. Wang, X. L. Feng, S. X. Du, K. Müllen and H.-J. Gao, *Appl. Phys. Lett.*, 2011, **99**, 153101.
- 49 A. J. Pollard, E. W. Perkins, N. A. Smith, A. Saywell, G. Goretzki, A. G. Phillips, S. P. Argent, H. Sachdev, F. Müller, S. Hüfner, S. Gsell, M. Fischer, M. Schreck, J. Osterwalder, T. Greber, S. Berner, N. R. Champness and P. H. Beton, *Angew. Chem. Int. Ed.*, 2010, **49**, 1.
- 50 S. Joshi, F. Bischoff, R. Koitz, D. Eciija, K. Seufert, A. P. Seitsonen, J. Hutter, K. Diller, J. I. Urgel, H. Sachdev, J. V. Barth and W. Auwärter, *ACS Nano*, 2014, **8**, 430.
- 51 F. Schulz, R. Drost, S. K. Hämmäläinen and P. Liljeroth, *ACS Nano*, 2013, **7**, 11121–11128.
- 52 P. Järvinen, S. K. Hämmäläinen, K. Banerjee, P. Häkkinen, M. Ijäs, A. Harju and P. Liljeroth, *Nano Lett.*, 2013, **13**, 3199–3204.
- 53 D. Jiang, M.-H. Du and S. Dai, *J. Chem. Phys.*, 2009, **130**, 074705.
- 54 B. Wang, M. L. Bocquet, S. Marchini, S. Günther and J. Winterlin, *Phys. Chem. Chem. Phys.*, 2008, **10**, 3530.
- 55 B. Wang, S. Günther, J. Winterlin and M. L. Bocquet, *New J. Phys.*, 2010, **12**, 043041.
- 56 B. Borca, S. Barja, M. Garnica, D. Sanchez-Portal, V. Silkin, E. V. Chulkov, C. F. Hermanns, J. J. Hinarejos, A. L. Vázquez de Parga, A. Arnau, P. M. Echenique and R. Miranda, *Phys. Rev. Lett.*, 2010, **105**, 036804.
- 57 J. P. Perdew, K. Burke and M. Ernzerhof, *Phys. Rev. Lett.*, 1996, **77**, 3865.
- 58 S. Grimme, *J. Comp. Chem.*, 2006, **27**, 1787.
- 59 G. Kresse and J. Hafner, *Phys. Rev. B*, 1993, **47**, 558.
- 60 G. Kresse and D. Joubert, *Phys. Rev. B*, 1999, **59**, 1758.
- 61 M. Methfessel and A. T. Paxton, *Phys. Rev. B*, 1989, **40**, 3616.
- 62 J. Tersoff and D. R. Hamman, *Phys. Rev. Lett.*, 1983, **50**, 1998.
- 63 M. J. Frisch, G. W. Trucks, H. B. Schlegel, G. E. Scuseria, M. A. Robb, J. R. Cheeseman, G. Scalmani, V. Barone, B. Mennucci, G. A. Petersson, H. Nakatsuji, M. Caricato, X. Li, H. P. Hratchian, A. F. Izmaylov,

- J. Bloino, G. Zheng, J. L. Sonnenberg, M. Hada, M. Ehara, K. Toyota, R. Fukuda, J. Hasegawa, M. Ishida, T. Nakajima, Y. Honda, O. Kitao, H. Nakai, T. Vreven, J. A. Montgomery, Jr., J. E. Peralta, F. Ogliaro, M. Bearpark, J. J. Heyd, E. Brothers, K. N. Kudin, V. N. Staroverov, R. Kobayashi, J. Normand, K. Raghavachari, A. Rendell, J. C. Burant, S. S. Iyengar, J. Tomasi, M. Cossi, N. Rega, J. M. Millam, M. Klene, J. E. Knox, J. B. Cross, V. Bakken, C. Adamo, J. Jaramillo, R. Gomperts, R. E. Stratmann, O. Yazyev, A. J. Austin, R. Cammi, C. Pomelli, J. W. Ochterski, R. L. Martin, K. Morokuma, V. G. Zakrzewski, G. A. Voth, P. Salvador, J. J. Dannenberg, S. Dapprich, A. D. Daniels, . Farkas, J. B. Foresman, J. V. Ortiz, J. Cioslowski and D. J. Fox, *Gaussian 09 Revision A.1*, Gaussian Inc. Wallingford CT 2009.
- 64 A. D. Becke, *J. Chem. Phys.*, 1993, **98**, 5648–5652.
- 65 S. Marchini, S. Günther and J. Wintterlin, *Phys. Rev. B*, 2007, **76**, 075429.
- 66 D. Martocchia, P. R. Willmott, T. Brugger, M. Björck, S. Günther, C. M. Schlepütz, A. Cervellino, S. A. Pauli, B. D. Patterson, S. Marchini, J. Wintterlin, W. Moritz and T. Greber, *Phys. Rev. Lett.*, 2008, **101**, 126102.
- 67 T. Brugger, S. Günther, B. Wang, J. H. Dil, M.-L. Bocquet, J. Osterwalder, J. Wintterlin and T. Greber, *Phys. Rev. B*, 2009, **79**, 045407.
- 68 To better compare the simulated STM images with the experimental results, the topography of TCNQ and F4-TCNQ adsorbed on gr./Ru(0001) shown in Fig. 1(b,c) have been measured for the individual species deposited separately over gr./Ru(0001).
- 69 D. Maccariello, M. Garnica, M. A. Niño, C. Navío, P. Perna, S. Barja, A. L. Vázquez de Parga and R. Miranda, *Chem. Mater.*, 2014, DOI:10.1021/cm5005467.
- 70 U. Fano, *Phys. Rev.*, 1961, **124**, 1866–1878.
- 71 J. B. Neaton, M. S. Hybertsen and S. G. Louie, *Phys. Rev. Lett.*, 2006, **97**, 216405.
- 72 R. F. W. Bader, *Atoms in molecules: A quantum theory*, Oxford University Press, Oxford, 1990.
- 73 W. Tang, E. Sanville and G. Henkelman, *J. Phys.: Condens. Matt.*, 2009, **21**, 1.
- 74 M. Garnica, D. Stradi, F. Calleja, S. Barja, C. Díaz, M. Alcamí, A. Arnau, A. Vázquez de Parga, F. Martí and R. Miranda, *Nano Lett.*, 2014, **14**, 4560.
- 75 R. O. Jones and O. Gunnarson, *Rev. Mod. Phys.*, 1989, **61**, 689.
- 76 This value agrees well with that reported in literature ($\Delta E = -3.22$ eV) using multiconfigurational quantum chemistry methods⁸¹.
- 77 H. Winter, *Phys. Rep.*, 2002, **367**, 387–582.
- 78 T. C. Tseng, C. Urban, Y. Wang, R. Otero, S. L. Tait, M. Alcamí, D. Écija, M. Trelka, J. M. Gallego, N. Lin, M. Konuma, U. Starke, A. Nefedov, A. Langner, C. Wöll, M. A. Herranz, F. Martín, N. Martín, K. Kern and R. Miranda, *Nat. Chem.*, 2010, **2**, 374.
- 79 L. Romaner, G. Heimel, J.-L. Brédas, A. Gerlach, F. Schreiber, R. L. Johnson, J. Zegenhagen, S. Duhm, N. Koch and E. Zojer, *Phys. Rev. Lett.*, 2007, **99**, 256801.
- 80 Note that, albeit the most stable configuration of the doubly charged TCNQ dimer is the open-shell triplet, the calculations presented in the manuscript have been carried out for the slightly less stable close-shell singlet ($\Delta E = +316$ meV), because performing non spin-polarized calculations results in a smoother PES. However, the results obtained by considering the 2D PES of the open-shell triplet of both the doubly-charge TCNQ and the doubly charged F4-TCNQ dimers are qualitatively identical.
- 81 B. Milián, R. Pou-Amérgo, R. Viruela and E. Ortí, *Chem. Phys. Lett.*, 2004, **391**, 148.